Interplay disorder-interaction in one dimensional quantum models

J.-L. Pichard, D. Weinmann, S. De Toro Arias, R.A. Jalabert, P. Schmitteckert, X. Waintal, A. Wobst

Annalen
der Physik

Interplay disorder-interaction in one dimensional quantum models

Jean-Louis Pichard[1], **Dietmar Weinmann**[2], **Samuel De Toro Arias**[1], **Rodolfo A. Jalabert**[3], **Peter Schmitteckert**[1,3], **Xavier Waintal**[1], **and André Wobst**[2]

[1] CEA, Service de Physique de l'Etat Condensé, Centre d'Etudes de Saclay, F-91191 Gif-sur-Yvette, France

[2] Institut für Physik, Universität Augsburg, 86135 Augsburg, Germany

[3] Institut de Physique et Chimie des Materiaux de Strasbourg, 23 rue de Loess, 67037, Strasbourg cedex, France

Received 6 October 1998

Abstract. We show that the crossover from the weak interaction limit towards the strong interaction limit may be accompanied by a delocalization effect in one dimensional disordered quantum models. The spin degrees of freedom are frozen and the spatial wave functions remain symmetric or antisymmetric when the strength U of a short range interaction is varied. The study concerns the excited states for two interacting particles and the ground state for a finite density of carriers.
First, for two particles in a chain of length L, we establish a duality transformation mapping the behavior at weak U onto the behavior at strong U. For intermediate U, the mixing of the one body states and the interaction induced delocalization effect are maximum. Furthermore, if $L \approx L_1$ (the one particle localization length), the system becomes weakly chaotic with critical spectral statistics. This weak chaos is related to the multifractality of the interaction matrix. For two particles starting close to each other, localization is reached in two steps. Before the time t_1 necessary to propagate over L_1, U de-favors the propagation. On the contrary, U favors a very slow delocalization after t_1, characterized by a $\log(t)$ spreading of the center of mass. Similarly, the curvatures of the energy levels with respect to an enclosed magnetic flux decrease as a function of U for $L < L_1$ and increase for $L > L_1$. The changes of the curvatures can be described by a conductance-like single scaling parameter.
Second, using the density renormalization group algorithm, we have studied the ground state energy of a finite density of spinless fermions and its change under twisted boundary conditions. For a large disorder, a charge reorganization is induced by the interaction: When the system becomes instable between the inhomogeneous configuration driven by the random potential (Anderson insulator) and the homogeneous one driven by repulsive interactions (Mott insulator), the ground state sensitivity can be enhanced by orders of magnitude. In contrast, no enhancement occurs at weaker disorder, when there are many particles on a scale L_1.

Keywords: Interaction, Disordered systems, Delocalization

The competition between electron-electron interaction and one body kinetic energy in disordered systems is a fundamental problem of permanent interest [1]. We denote by U, t and W the parameters characterizing the interaction, the one body kinetic energy and the fluctuations of the random potential for a d-dimensional system of size

L. When U is small, the N-body eigenstates are close to the symmetrized products of one body states (Slater determinants for spinless fermions) which contain the effects of t and W completely. The effect of U can be treated as a perturbation, yielding a mixing of those symmetrized products. When U increases, the consequence of this mixing is that an increasing number of one body states is needed to describe the exact N-body states. If the one body states are localized by the disorder, delocalization in real space results from this mixing. This is why the interaction can induce in certain cases metallic behavior in a system which would be an insulator otherwise. When U is large and dominates, one can get on the contrary a correlated insulator which might be metallic at weaker interaction. A Wigner crystal pinned by disorder is a good example of such an interaction-induced insulator.
For one dimensional disordered quantum systems, we show that the crossover from the weak interaction limit towards the strong interaction limit is accompanied by a delocalization effect in two cases: two electrons of high energy with opposite spins (the orbital part of the wave-function is symmetric as in the case of two bosons) and the ground state of spinless fermions at half filling.

1 Two interacting particles

We summarize in this section the main conclusions of a series of recent works [2, 3, 4, 5] dealing with two interacting particles (TIP) described by a tight-binding Hamiltonian

$$H = H_1 \otimes \mathbf{1} + \mathbf{1} \otimes H_1 + H_{\rm int} \, . \tag{1}$$

H_1 describes one particle in a disordered chain with L sites and reads

$$H_1 = \sum_{n=1}^{L} \Big(-t|n+1\rangle\langle n| - t^*|n\rangle\langle n+1| + V_n|n\rangle\langle n| \Big) \, , \tag{2}$$

where $|n\rangle$ is a Wannier function localized at site n. In the case of periodic boundary conditions the chain is closed to a ring, setting $|n\rangle \equiv |n+L\rangle$. The disorder is modeled by random on-site energies V_n which are distributed uniformly inside the interval $[-W : W]$. The nearest neighbor hopping matrix elements $t = t_0 \equiv 1$ set the energy scale.
We assume Hubbard-like on-site interaction with strength U between the two particles given by

$$H_{\rm int} = \sum_{n=1}^{L} U|nn\rangle\langle nn| \, . \tag{3}$$

Here, $|mn\rangle$ means $|m\rangle \otimes |n\rangle$. We restrict ourselves to the case of two fermions with opposite spins. We have only to consider symmetric "boson-like" TIP states and the dimension of the Hilbert space is $M = L(L+1)/2$. A complete basis for the symmetric configuration space part of the states is given by

$$|mn\rangle_s = \frac{1}{\sqrt{2}}(|mn\rangle + |nm\rangle) \quad \text{for} \quad m \neq n \quad \text{and} \quad |nn\rangle_s = |nn\rangle \, . \tag{4}$$

For the main sub-band of states centered around $E = 0$, both in the limits where $U = 0$ (free bosons) and $U = \infty$ (hard-core bosons), the two body states can be described in terms of two one body states. We use a duality transformation $U \to at^2/U$ to map

the small U-limit onto the large U-limit ($a \approx \sqrt{24}$). We first prove that the lifetimes of the free boson states and of the hard-core boson states are equal at the fixed point U_c of the duality transformation. At U_c one has the maximum mixing of the one body states by the interaction and the enhancement factor [6, 7, 8] is maximum for the two particle localization length L_2. Far from U_c, L_2 is smaller and satisfies the duality relation. $L_2 \to L_1$ (the one particle localization length) both for $U \to 0$ and $U \to \infty$. The study of the signature of this duality transformation on the spectral fluctuations is very interesting. For $E = 0$, taking $L = L_1$ and increasing U, one gets two thresholds defining a range of interaction $U_F \leq U \leq U_H$. Outside this range, the levels are almost uncorrelated. Inside this range, the level repulsion is maximum, but does not reach the universal Wigner-Dyson (W-D) repulsion. The two particle system is not fully chaotic, but exhibits a weak chaos which is not arbitrarily situated between Poisson (integrable) and Wigner (chaos). The spacing distribution $p(s)$ between consecutive energy levels and the statistics $\Sigma_2(E)$ (variance of the number of energy levels inside an energy interval E) are characteristic of the third known universality class [9]. One finds $p(s) \approx 4s \exp(-2s)$ and $\Sigma_2(E) \approx 0.16 + 0.41E$ for periodic boundary conditions. This is very close, if not identical, to the distributions found in many "critical" one body systems, such as an electron in a 3d random potential at the mobility edge or in certain pseudo-integrable quantum billiards. Furthermore, $p(s)$ saturates to $4s \exp(-2s)$ for $U \approx U_c$ only when the ratio $1 \leq L_1/L \leq 10$. We conclude that a local interaction can never drive the two particle system to full quantum chaos with Wigner-Dyson statistics in one dimension, but can at most yield weak critical chaos in a certain domain of interaction and of the ratios L_1/L. We show in addition that this weak chaos is accompanied by multifractal wave-functions.

While one-particle wave-functions in two dimensions have a multifractal character within their localization domains [10], the elastic mean free path and the localization length coincide in one dimension, preventing a single one particle wave function to be multifractal over a significant range of scales. When one writes the two-particle Hamiltonian in the basis built from the one particle states (eigenbasis without interaction), the interaction matrix elements coupling a free boson state to the others have not only a broad and non Gaussian [11] distribution, but defines a multifractal measure in the free boson eigenbasis, which is at the origin of critical statistics and multifractal wave-functions. Moreover, since the obtained Rényi dimensions do not depend on L_1, simple power laws describe how the moments scale with the characteristic length L_1 of the one body problem. For a size $L \approx L_1$, we show that, contrary to previous assumptions, the two body eigenstates without interaction directly coupled by the square of the hopping terms have not a density of the order of the two body density $\rho_2(L_1) \propto L_1^2$, but a smaller density $\rho_2^{\text{eff}}(L_1) \propto L_1^{f(\alpha(q=2))}$ with $f(\alpha(q=2)) \approx 1.75$.

The properties of the two body problem in one dimension have interesting consequences for the mobility of the particles. This can be observed in the real-time development of wave packets representing two particles initially being localized in two neighboring sites in the middle of a disordered chain of size $L \gg L_1$. The TIP-dynamics is characterized by two times t_1 and t_2, where a scale of order of L_1 and L_2 is explored, respectively. Between t_1 and t_2, the spreading of the center of mass spreads with an extremely slow $\log(t)$-law, quite different from a previously assumed diffusion law. This is consistent with the absence of full quantum chaos with Wigner-Dyson spectral statistics. Another important phenomenon illustrated by this study is the inversion of the effect of the interaction when the ballistic motion ($t < t_1$) becomes

sub-diffusive ($t_1 < t < t_2$): First U de-favors the ballistic propagation before having an opposite delocalizing effect.
This is directly related to the behavior of the level curvatures with respect to an enclosed flux in ring geometries. Since the latter are known to be closely related [12, 13] to the conductance in the case of one-particle energy levels in disordered mesoscopic systems, one can suspect that they are a measure of the mobility of the particles also in the interacting two body case. Very recently, Akkermans and Pichard [14] have studied the connection between spectral correlations and level curvatures for two interacting particles. They predicted that the curvatures should be enhanced by interactions in localized and reduced in metallic samples. In a numerical study, we have unambiguously confirmed this prediction. Furthermore, our data suggest that the effect of the interaction on curvatures exhibits one-parameter scaling. The scaling parameter is closely related to the non-interacting conductance.

1.1 Duality small $U \leftrightarrow$ large U

Denoting $|\alpha\rangle$ the one body eigenstate of energy ϵ_α and the amplitude $\langle n|\alpha\rangle = \Psi_\alpha(n)$, only two one body states $|\alpha\rangle$ and $|\beta\rangle$ are necessary to describe a free boson state $|fb\rangle = |\alpha\beta\rangle$ with components

$$\langle n_1 n_2|fb\rangle = (\Psi_\alpha(n_2)\Psi_\beta(n_1) + \Psi_\alpha(n_1)\Psi_\beta(n_2))/\sqrt{2}. \tag{5}$$

In this free boson basis, the interaction matrix elements $\langle\alpha\beta|H_{\rm int}|\gamma\delta\rangle = 2UQ^{\gamma\delta}_{\alpha\beta}$ where

$$Q^{\gamma\delta}_{\alpha\beta} = \sum_{n=1}^{L} \Psi_\alpha(n)\Psi_\beta(n)\Psi_\gamma(n)\Psi_\delta(n). \tag{6}$$

As noticed in Ref. [15], there is a useful representation for an on-site interaction $U \to \pm\infty$, composed by a small set of $L_{\rm M} = L$ "molecular" states $|nn\rangle$ and by a large set of $L_{\rm H} = L(L-1)/2$ hard core boson states $|hc\rangle$ built from re-symmetrized Slater determinants with components

$$\langle n_1 n_2|hc\rangle = (\Psi_\alpha(n_2)\Psi_\beta(n_1) - \Psi_\alpha(n_1)\Psi_\beta(n_2))\mathrm{sgn}(n_2 - n_1)/\sqrt{2}\,. \tag{7}$$

The re-symmetrization is insured by the function $\mathrm{sgn}(x) := x/|x|$. For hard wall boundaries, the same one body states $|\alpha\rangle$ and $|\beta\rangle$ are used for $|fb\rangle$ and $|hc\rangle$. In this basis, the two body Hamiltonian $\mathcal{H}$ has the structure

$$\mathcal{H} = \begin{bmatrix} H_{\rm M} & H_{\rm C} \\ H_{\rm C}^T & H_{\rm H} \end{bmatrix}. \tag{8}$$

$H_{\rm M}$ and $H_{\rm H}$ are $L_{\rm M} \times L_{\rm M}$ and $L_{\rm H} \times L_{\rm H}$ diagonal matrices with entries $U + 2V_n$ and $\epsilon_{hc} = \epsilon_\alpha + \epsilon_\beta$, respectively. $H_{\rm M}$ and $H_{\rm H}$ are coupled by a rectangular matrix $H_{\rm C}$ resulting from the kinetic terms $\sqrt{2}\,t\sum_{n=1}^{L-1}(|n,n+1\rangle\langle n,n| + |n,n\rangle\langle n,n+1| + \mathrm{h.c.})$ of $\mathcal{H}$. The matrix elements of $H_{\rm C}$ are equal to $\sqrt{2}\,t\left(\Psi_\beta(n)\hat{D}\Psi_\alpha(n) - \Psi_\alpha(n)\hat{D}\Psi_\beta(n)\right)$, where $\hat{D}\Psi_\alpha(n) := \Psi_\alpha(n+1) - \Psi_\alpha(n-1)$. The states $|hc\rangle$ of energy $\epsilon_{hc} \approx 0$ are coupled by a term of order t to the few states $|nn\rangle$ of energy $\approx U$. Their lifetime becomes infinite when $U \to \pm\infty$.

Projecting an eigenstate $|A\rangle$ of energy E_A onto the states $|nn\rangle$ and $|hc\rangle$

$$|A\rangle = \sum_{n=1}^{L_{\rm M}} c_A^n |nn\rangle + \sum_{hc=1}^{L_{\rm H}} c_A^{hc} |hc\rangle \,, \tag{9}$$

one finds the relation

$$\begin{bmatrix} H_{\rm M} + J_{\rm M}(E_A) & 0 \\ 0 & H_{\rm H} + J_{\rm H}(E_A) \end{bmatrix} \begin{bmatrix} C_A^{\rm M} \\ C_A^{\rm H} \end{bmatrix} = E_A \begin{bmatrix} C_A^{\rm M} \\ C_A^{\rm H} \end{bmatrix},$$

which holds for arbitrary U. $C_A^{\rm M}$ and $C_A^{\rm H}$ are vectors of $L_{\rm M}$ components c_A^n and $L_{\rm H}$ components c_A^{hc}, respectively. The matrix $J_{\rm H}(E_A)$ has $L_{\rm H}^2$ elements of the form

$$J_{\rm H}(E_A, hc, \tilde{hc}) = \sum_{n=1}^{L_{\rm M}} \frac{\langle hc|H_{\rm C}|nn\rangle\langle nn|H_{\rm C}|\tilde{hc}\rangle}{U + 2V_n - E_A}. \tag{10}$$

Considering the main sub-band of states with energy $E_A \approx 0$, resulting from the mixing by a perturbation of order t^2/U of a few states $|hc\rangle$ for which $J_{\rm H}(E_A)$ can be simplified. Assuming $W, t \ll U$ and $U + 2V_n - E_A \approx U$, one has to evaluate $\sum_{n=1}^{L} \langle hc|H_{\rm C}|nn\rangle\langle nn|H_{\rm C}|\tilde{hc}\rangle$. This expression is composed of 12 sums over n, each of them having the form

$$\tilde{Q}_{\alpha\beta}^{\gamma\delta} = \sum_{n=1}^{L} \Psi_\alpha(n)\Psi_\beta(n')\Psi_\gamma(n)\Psi_\delta(n'') \tag{11}$$

with various combinations of $n', n'' = n \pm 1$. Therefore $\tilde{Q}_{\alpha\beta}^{\gamma\delta}$ is not exactly equal to the $Q_{\alpha\beta}^{\gamma\delta}$ occuring around the free boson limit. However, this difference should not be statistically relevant and if one neglects it, one finds

$$J_{\rm H}(E_A, hc, \tilde{hc}) \approx \pm 2(24)^{1/2} \frac{t^2}{U} Q_{\alpha\beta}^{\gamma\delta}. \tag{12}$$

This establishes the duality transformation $U \to a(t^2/U)$ for $E \approx 0$ which maps the distribution of the coupling terms between the $|fb\rangle$ when U is small onto the distribution of the coupling terms between the $|hc\rangle$ when U is large. The constant $a = \sqrt{24}$ if one has $U + 2V_n - E_A \approx U$ for every V_n.
To illustrate this duality around the fixed point $U_{\rm c} = (24)^{1/4}t$, we have numerically calculated the average over the disorder of the local density of states

$$\rho_A(E) = \sum_{\alpha\beta} |c_A^{\alpha\beta}|^2 \delta(E + E_A - \epsilon_\alpha - \epsilon_\beta) \tag{13}$$

for $L = L_1$ and $E_A \approx 0$. We have observed that $\langle \rho_A(E) \rangle$ can be fitted by a Lorentzian curve of width Γ_0 (if $\alpha\beta$ denotes the states $|fb\rangle$) or Γ_∞ (if $\alpha\beta$ denotes the states $|hc\rangle$). The dependence of Γ_0 and Γ_∞ on the interaction strength will be shown in Fig. 2.
In order to quantitatively understand the broadening of the states due to the interaction, it is very helpful to study in detail the properties of the matrix Q which depend on the one-body dynamics in the random potential.

1.2 Multifractality of the interaction matrix and weak critical quantum chaos

In the free boson eigenbasis, the system Hamiltonian is made of a diagonal matrix with essentially uncorrelated entries $\epsilon_\alpha + \epsilon_\beta$ plus a perturbation induced by the interaction and coupling the free boson states. If this perturbation was essentially an unstructured Gaussian matrix, the problem would consist of a Poisson diagonal matrix plus a GOE perturbation. In such a case, the perturbation would drive the system to full quantum chaos with GOE Wigner-Dyson spectral statistics. We will show that this is not the case. The most rigid spectrum that the interaction can induce exhibits critical statistics as the one particle problem at the mobility edge (where the eigenfunctions are known to be multifractal) or as in certain pseudo-integrable billiards. This means that the perturbation cannot be simplified by a GOE matrix in the free boson eigenbasis, but should have a more complex structure yielding critical statistics, and not GOE Wigner Dyson spectral rigidity. This is why we should first study the Q-matrix. We summarize a few evaluations of the second moment ($q = 2$) of $Q^{\gamma\delta}_{\alpha\beta}$ which have been previously used. Case (i): The one body Hamiltonian is described by random matrix theory (RMT). The statistical invariance under orthogonal transformations $O(M)$ implies that $\langle (Q^{\gamma\delta}_{\alpha\beta})^2 \rangle \approx 1/M^3$ where M is the number of one body states. Case (ii): The system is a disordered conductor of conductance g. An estimate [16] based on perturbation theory gives $\langle (UQ^{\gamma\delta}_{\alpha\beta})^2 \rangle \propto (\Delta/g)^2$. Since the one particle mean level spacing $\Delta \propto 1/M$, this perturbative result coincides with the previous RMT results if one takes $M \equiv g^2$. Moreover, it is valid only if all the one particle states appearing in Eq.(6) are taken from a sequence of g consecutive levels in energy. Otherwise, $Q^{\gamma\delta}_{\alpha\beta}$ can be neglected. Case (iii): The system is a disordered insulator. Shepelyansky [6] in his first study of the two interacting particles (TIP), assumes a RMT behavior for the $M = L_1^d$ components of the wave function inside the localization domain, and neglects the exponentially small components outside this domain. When the dimension $d = 1$, one gets a term $(Q^{\gamma\delta}_{\alpha\beta})^2 \approx 1/L_1^3$ for the terms coupling a TIP state $|\alpha\beta>$ to L_1^2 TIP states $|\gamma\delta>$. This estimate for $g < 1$ differs from the one valid when $g > 1$ under two important aspects: not only $M \approx L_1^d$ instead of g^2, but the condition for a large hopping is entirely different. In the insulator, a large hopping term is not given by four one particle states close in energy, but by four states close in real space, i.e. located inside the same localization domain. Ponomarev and Silvestrov have criticized [15] this estimate, using an approximate description of a localized state for weak disorder. They note that the density of TIP states coupled by the interaction is sensibly smaller.

For a more accurate study of $Q^{\gamma\delta}_{\alpha\beta}$ in one dimension, we numerically calculated the matrix elements using Eq.(6) and numerical diagonalization of the one particle Hamiltonian. $Q^{\gamma\delta}_{\alpha\beta}$, for fixed α and β is a two-dimensional object which is not defined in the real $2d$ space, but in the space of two one particle quantum numbers γ and δ. Those states $|\gamma>$ (and $|\delta>$) can be ordered in different ways: (a) spectral ordering by increasing eigenenergy, (b) spatial ordering by the location n_γ of their maximum amplitude, (c) momentum ordering if $W = 0$. The ordering (b) is meaningful only in the localized regime ($L > L_1$).

We first study the matrix element $Q^{\gamma\delta}_{\alpha_0\alpha_0}$, characterizing two electrons in the same state $|\alpha_0>$ hopping to an arbitrary state $|\gamma\delta>$. Hopping is very unlikely over scales larger than L_1. The L_1^2 large values of the hopping term are concentrated inside

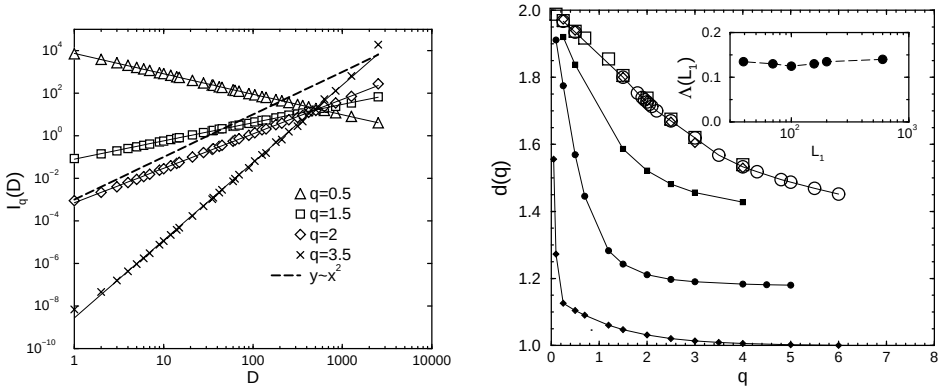

Fig. 1: Left: Power laws showing the relevance of a multifractal measure in the (γ, δ) two dimensional plane. $I_q(D)$ are calculated for a single sample with $L_1 = L = 2500$. α_0 in the bulk of the spectrum. The states $|\gamma\rangle$ and $\delta\rangle$ are ordered by increasing eigenenergy (ordering a). The dashed line corresponds to the RMT prediction (case (i)). Right: $d(q)$ with α_0 in the bulk of the spectrum using ordering (a) and after ensemble averaging. Filled symbols: $L = 240$ and $L_1 = \infty$ (diamonds), 25.10^4 (circles) and 2500 (squares). Open symbols: $L_1 = 70$ and $L = 960$ (diamonds), 480 (circles) and 240 (squares). Inset: the slope $\Lambda(L_1)$ showing that $d(q)$ is disorder independent for $q \leq 3$ and $L_1 < L$.

a square of size L_1^2 [2] for a given sample using ordering (b). Inside this square, a complex pattern occurs which reminds us another bi-dimensional object: the one particle wave function in a two dimensional disordered lattice. In analogy with the $2d$ one body problem, we now perform an analysis of the multifractality, not expecting that this multifractality will be valid in the whole (γ, δ) Hilbert space, but only in a limited but parametrically large domain.

We proceed as usual (see references [17, 18]) for the multifractal analysis. For L_1 and L fixed, we divide the plane (γ, δ) into $N_{\rm box} = (L/D)^2$ boxes of size D and calculate the ensemble averaged function for different values of q

$$I_q(D) = \sum_{i=1}^{N_{\rm box}} \left(\sum_{\gamma,\delta \in {\rm box}\ i} |Q^{\gamma\delta}_{\alpha_0\alpha_0}| \right)^q . \tag{14}$$

The existence of a multifractal measure defined in the (γ, δ)-plane by the interaction matrix elements is established in the next figures. In Fig.1, a single sample has been used and power laws $I_q(D) \propto D^{\tau(q)}$ are obtained over many orders of magnitude for different values of q. The corresponding Rényi dimensions $d(q) \equiv \tau(q)/(q-1)$ are shown in Fig. 1 for different L and L_1, using ordering (a) and ensemble averaging.

For an infinite L_1 (no disorder), the eigenstates are plane waves of momentum k_α and $Q^{\gamma\delta}_{\alpha\beta} \neq 0$ only if $k_\alpha + k_\beta - k_\gamma - k_\delta = 0$. This gives $d(0) = 2$ and $d(q > 0) = 1$ with ordering (c). The dimensions calculated with ordering (a) are close to this limit. For a finite L_1, $d(q)$ goes from the clean limit ($L << L_1$) to an L_1-independent regime when $L >> L_1$. In the crossover regime ($L \leq L_1$) the $d(q)$ depend on L_1. In the limit $L >> L_1$, the $d(q)$ (using orderings (a) or (b)) do not depend on L and L_1. For

$0 < q \leq 3$, $d(q) \approx 2 - \Lambda q$ with a slope $\Lambda \approx 0.135$. The L_1-independence of Λ is shown in the inset of Fig. 1 for $L_1 \leq L$ up to $L_1 = 600$.
A multifractal distribution has scaling behavior described by the $f(\alpha)$-spectrum, given by the relations

$$\alpha(q) = \frac{d\tau}{dq} \quad \text{and} \quad f(\alpha(q)) = \alpha(q) \cdot q - \tau(q) \,. \tag{15}$$

We obtain $f(\alpha(q)) \approx 2 - \Lambda q^2$ for $q \leq 3$, i.e. a parabolic shape $f(\alpha) = 2 - (\alpha - 2 - \Lambda)^2/(4\Lambda)$ around the maximum $2 + \Lambda$. We have mainly studied the first positive moments, since we are mainly interested by $f(\alpha(q = 2))$. Indeed, when one uses Fermi golden rule to calculate the interaction-induced decay of a non-interacting state, one needs to know the density of states directly coupled by the second moment ($q = 2$) of the hopping term. The fractal dimension of the support of this density is given by $f(\alpha(q = 2))$. For greater values of q, there are deviations around the parabolic approximation, indicating deviations around simple log-normal distributions. From a study of the large and small values of $|Q^{\gamma\delta}_{\alpha_0\alpha_0}|$, one can obtain $d(q \to \pm\infty)$. We find $d(+\infty) = 1.33$ and $d(-\infty) = 3.15$, giving the limits of the support of $f(\alpha)$.
We have also checked that our results for $Q^{\gamma\delta}_{\alpha_0\alpha_0}$ do not depend on the chosen α_0 and studied the general case where $|\alpha>$ and $|\beta>$ are not the same [2]. Using energy ordering (a) and imposing an energy separation $|\epsilon_\alpha - \epsilon_\beta| > \Delta(L_1)$ in order to have a good overlap between the fixed states α and β, we find also power law behaviors for $I_q(D)$. The corresponding dimensions $d(q)$ are characterized by a slope $\Lambda(\alpha \neq \beta) \approx \Lambda(\alpha = \beta)/2 \approx 0.065$. Therefore, the multifractal character of $Q^{\gamma\delta}_{\alpha\beta}$ is less pronounced when $|\alpha> \neq |\beta>$, but remains relevant.
As pointed out by Shepelyansky, the interaction induced hopping mixes nearby in energy TIP states $|\alpha\beta>$. The decay width Γ [8, 19, 20] of a TIP state $|\alpha\beta>$, built out from two one particle states localized within L_1, can be estimated using Fermi's golden rule. If one assumes RMT wave functions inside L_1 for the one particle states, (case (iii)) the $Q^{\gamma\delta}_{\alpha\beta} \approx \pm U \cdot L_1^{-3/2}$ couple the TIP state $|\alpha\beta>$ to all the TIP states $|\gamma\delta>$ inside L_1. Around the band center, they have a density $\rho_2(L_1) \propto L_1^2$ and Fermi golden rule gives

$$\Gamma(E \approx 0) \propto \frac{U^2}{L_1^3}\rho_2(L_1) = \frac{U^2}{L_1} \,. \tag{16}$$

However, not all the TIP states within the localization domains are equally coupled by the interaction. Since the square of the hopping terms appears in the golden rule, our multifractal analysis gives a reduced effective TIP density $\rho_2^{\text{eff}} \propto L_1^{f(\alpha(q=2))}$ which should replace the total TIP density $\rho_2(L_1)$. The resulting expression

$$\Gamma_{\alpha\beta} \propto \frac{U^2}{L_1^3} L_1^{f(\alpha(q=2))} \tag{17}$$

agrees with the direct numerical evaluation

$$\Gamma_{\alpha\beta} = U^2 \sum_{\gamma\delta} |Q^{\gamma\delta}_{\alpha\beta}|^2 \delta(\epsilon_\alpha + \epsilon_\beta - \epsilon_\gamma - \epsilon_\delta) \tag{18}$$

of the Golden rule decay [2] when $L \geq L_1$.
For $L \approx L_1$, one has $\rho_2^{\text{eff}}(L_1) \propto L_1^{1.75}$, instead of the total two body density $\rho_2 \propto L_1^2$. Therewith, Fermi's golden rule gives for the widths Γ_0 and Γ_∞ in the free boson and

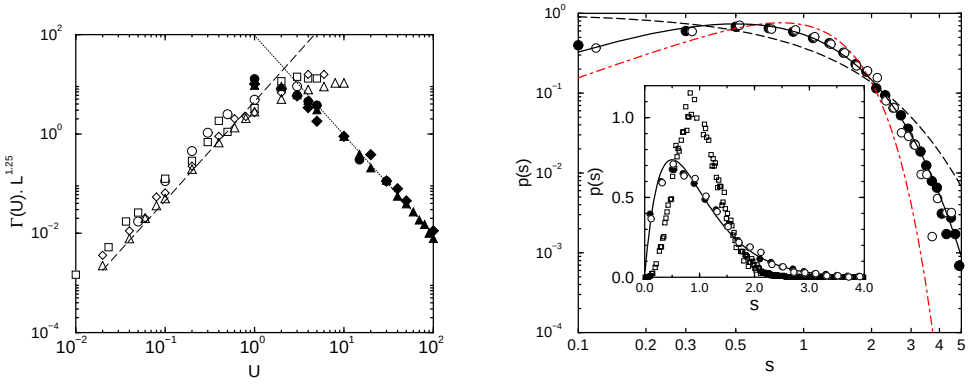

Fig. 2: Left: Γ_0 (open symbols) and Γ_∞ (filled symbols) for $L = 25$ (triangles), $L = 76$ (diamonds), $L = 150$ (squares) and $L = 200$ (circles). Dashed (dotted) lines are the Fermi golden rule expression of Eq.19. Right: TIP-$p(s)$ for $L = L_1 = 150$ and $U = 1$: Continuous, dotted and dashed lines correspond to the "Semi-Poisson", Wigner and Poisson distributions respectively. Full (empty) circles correspond to hard-wall (periodic) boundary conditions. Inset: TIP-$p(s)$ (circles $U = 1$) compared to the one particle $p(s)$ (squares) for $L = L_1 = 150$.

the hard core boson bases, at $L \approx L_1$

$$\Gamma_0 \approx 2\pi U^2 \frac{1}{L_1^3}\rho_2^{\rm eff}(L_1) \quad \text{and} \quad \Gamma_\infty \approx 2\pi \frac{24t^4}{U^2}\frac{1}{L_1^3}\rho_2^{\rm eff}(L_1)\,. \tag{19}$$

As shown in figure 2, the widths Γ obey the duality property $\Gamma_0(U) = \Gamma_\infty(\sqrt{24}t^2/U)$, and are described by the above golden rule approximations. When $U \approx U_{\rm c}$, the lifetime of the free boson states is equal to the one of the hard core boson states. Signatures of this duality have been observed in the level statistics (see Fig. 4 of Ref. [19]) and in a study of the pair localization length L_2 [21]. However, deviations from $a = \sqrt{24}$ occurred. This might be due to rather small values of L_1 and thus a relatively large number L of molecular states as compared to the total number of states $\sim LL_1$ feeling the interaction.

When U increases, the statistical ensemble associated to the two particle system exhibits a crossover from one preferential basis (the free boson basis) to another preferential basis (the hard core boson basis). At $U_{\rm c}$, the statistical ensemble is in the middle between the two preferential bases, the mixing of the one body states is maximum, and the localization length L_2 therefore is maximum. When $E = 0$ and U varies, a transition occurs in the two body spectrum in 1d which is somewhat reminiscent of the one body case in 3d when $E = 0$ and W varies and the question whether or not the spectral fluctuations are of the same kind in the vicinity of the threshold deserves to be investigated.

Before showing the results, two arguments can be mentioned: (i) A multifractal Q-matrix is incompatible with Wigner-Dyson level repulsion in 1d. The states $|fb\rangle$ or $|hc\rangle$ are directly coupled by U or t^2/U to an effective density $\rho_2^{\rm eff} < \rho_2$. Therefore, nearest neighbors in energy are very likely uncorrelated, enhancing the probability to find level spacings small compared to their average. (ii) Looking at Eq. 3, one may

assume that a broad distribution of the matrix elements of $H_{\rm M}$ may yield a single dominant coupling term. This allows us to consider that the states $|hc\rangle$ are mainly coupled via a few states $|nn\rangle$. This is not far from the case discussed by Bohr and Mottelson [22] (coupling via a single state) where the consecutive levels E_A of $\mathcal{H}$ satisfy the conditions $\epsilon_{hc} < E_A < \epsilon_{hc+1} < E_{A+1}$, ϵ_{hc} being the consecutive levels of $H_{\rm H}$. Since the statistics of $H_{\rm H}$ is essentially Poissonian, this forbids to have the Wigner-Dyson rigidity for the E_A. The most rigid spectrum would be achieved by putting the E_A exactly in the middle of two consecutive ϵ_{hc}. It is straightforward to find that $p(s)$ would then be equal to $p_{\rm c}(s) = 4s\exp(-2s)$. This "semi-Poisson" distribution, where $p_{\rm c}(s) \propto s$ for $s \ll 1$ (as the Wigner surmise $p_{\rm W}(s) = (\pi/2)s\exp(-\pi s^2/4)$), and which decays as $\exp(-s)$ for $s \gg 1$ (as the Poisson distribution $p_{\rm P}(s)$), characterizes weak chaos in critical systems [23].
These observations lead us to study $p(s)$ as a function of U and of the ratio L_1/L around $E = 0$ [3]. For $U = 1$ and $L = L_1 = 150$, the spacing distribution $p(s)$ is shown in Fig. 2, in good agreement with the "semi-Poisson" distribution. In the inset, one can see that this is specific to the two particle problem, and does not characterize the single particle spectrum for the same chain of size L_1.
We now study the domain of validity for weak chaos and universal critical statistics. To measure the deviation of $p(s)$ from the $P_{\rm P}(s)$ or $P_{\rm W}(s)$, we use the functional

$$\eta(U) = \frac{\int_0^b {\rm d}s(p(s) - p_{\rm W}(s))}{\int_0^b {\rm d}s(p_{\rm P}(s) - p_{\rm W}(s))} \tag{20}$$

with $b = 0.4729$. A Poisson spectrum gives $\eta = 1$, a Wigner-Dyson spectrum gives $\eta = 0$ and "semi-Poisson" corresponds to $\eta_c \approx 0.386$.
First, we vary U, imposing the relation $L = L_1$. We assume L_1 to be given by the weak disorder formula $L_1 \approx 25/W^2$. In the limits $U \to 0$ and $U \to \infty$, the TIP-levels are given by $\epsilon_{fb} = \epsilon_{hc} = \epsilon_\alpha + \epsilon_\beta$ which are uncorrelated (at least on energy scales smaller than the one particle level spacing Δ_1). This gives $p_{\rm P}(s)$ for the TIP-spectrum. One can see in fig. 3 that $p(s)$ deviates for small U and t^2/U from $p_{\rm P}(s)$ observed at $U = 0$ and $U = \infty$. $\eta(U)$ exhibits a plateau ($U_{\rm F} < U < U_{\rm H}$) at the value $\eta_{\rm c} \approx 0.386$ which characterizes $p_{\rm c}(s)$). We suggest that $U_{\rm F}$ and $U_{\rm H}$ are given by the conditions which hold [20] for systems in which there is no coupling term between consecutive energy levels. In agreement with the general picture developed in Ref. [20] (see also Ref. [24]), the threshold appears when the strength of the coupling terms becomes of the order of the spacing $1/\rho_2^{\rm eff}$ of the directly coupled levels. This gives $2U_{\rm F}/L_1^{3/2} \approx 4t/L_1^{1.75}$ and $2\sqrt{24}t^2/(U_{\rm H}L_1^{3/2}) \approx 4t/L_1^{1.75}$, respectively, and seems to account for the size of the plateau of the curve $\eta(U)$. This favors a line of critical points rather than an isolated point when the condition $L = L_1$ is imposed. A study of the spectral rigidity Σ_2 leads to the same conclusions [3].
At fixed interaction strength $U = 1.25$ which yields the maximum mixing, one finds the critical statistics for $1 \leq L_1/L \leq 10$ [3]. The critical correlations are suppressed both in the clean limit $L \ll L_1$ and in the localized limit $L \gg L_1$. The critical statistics is accompanied by multifractal two body wave-functions [3].

1.3 Real-time development of wave-packets

In order to understand the relevance of the above results for the two-particle dynamics, it is very instructive to consider the real-time dynamics of wave-packets in

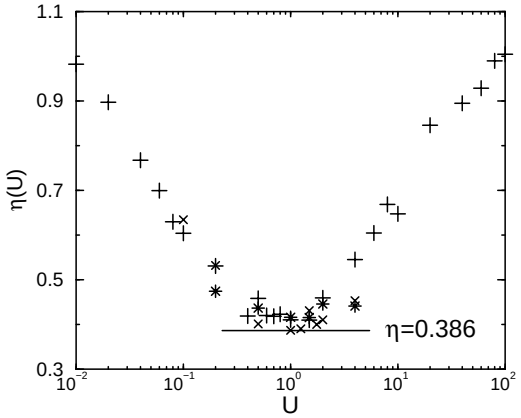

Fig. 3: Weak chaos and interaction for $L = L_1$: Crosses, pluses and stars represent $\eta(U)$ for $L = 100$, $L = 150$ and $L = 200$, respectively.

large systems [4] (when the system size L is much larger than both, L_1 and the pair localization length L_2, finite size effects can be neglected).
This illustrates the TIP delocalization phenomenon when $t \to \infty$. To study in detail the time dependence of the size of the wave-packet yields interesting additional informations about the quantum motion. First, a ballistic regime ($t < t_1$) appears in which U de-favors propagation. By chosing different initial wave packets, one finds signatures of the duality transformation discussed in section 1.1. A sub-diffusive regime ($t_1 < t < t_2$) where interaction favors a slow TIP propagation follows.
To study the motion of two electrons with opposite spins in a one dimensional Anderson tight binding model with on site interaction, we numerically solve the discretized TIP Schrödinger equation

$$\frac{i}{2\epsilon}\left(|\psi(t+\epsilon)\rangle - |\psi(t-\epsilon)\rangle\right) = \mathcal{H}|\psi(t)\rangle\,. \tag{21}$$

To solve Eq.(21), we use an automaton-like algorithm[25], which relies on a formulation of discrete scalar wave propagation in an arbitrary inhomogeneous medium by the use of elementary processes obeying a discrete Huygens' principle and satisfying fundamental symmetries, as described in Ref. [25]. Our algorithm avoids the direct discretization procedure and incorporates the symmetries underlying the Anderson model at the lowest stage of the construction. As a consequence the algorithm preserves the unitarity of the dynamics, insuring the normalization of the wave-function at all times, $\sum_{n_1,n_2} |\psi_{n_1,n_2}(t)|^2 = 1$, up to a small correction of order ϵ^2. Besides, the construction is optimized for implementing the algorithm on massively parallel machines. The numerical simulations have been performed for a time step $\epsilon = 0.05$ on a 16K processor Connexion Machine. Given a value of the disorder strength W and a disorder configuration, the wave-function has been calculated for chains of length as large as $L = 1024$ and up to a maximum of 10^6 units of time.
In this section, all the energies are given in units of $1/\epsilon$. The times are then expressed in the corresponding units (ϵ). The sites are labeled from $-L/2$ to $+L/2$, such that

the site $n = 0$ is located in the middle of the chain. The initial condition corresponds to

$$\psi_{n_1,n_2}(0) = \psi_{n_1,n_2}(\epsilon) = \frac{1}{\sqrt{2}}(\delta_{n_1,0}\delta_{n_2,\rho_0} + \delta_{n_2,0}\delta_{n_1,\rho_0})$$

where $\langle n_1 n_2|\psi(t)\rangle = \psi_{n_1,n_2}(t)$. When ϵ is small enough, the discrete time Eq.(21) has the same physical content than its continuous version.
To study the spreading $R(t)$ of the center of mass and the size $\rho(t)$ of the pair, we use the following functions:

$$R(t) = \left(\sum_{n_1,n_2} |\psi_{n_1,n_2}(t)|^2 \frac{(n_1 - \bar{n}_1 + n_2 - \bar{n}_2)^2}{2}\right)^{1/2} \quad (22)$$

$$\rho(t) = \left(\sum_{n_1,n_2} |\psi_{n_1,n_2}(t)|^2 \frac{(n_1 - \bar{n}_1 - n_2 + \bar{n}_2)^2}{2}\right)^{1/2} \quad (23)$$

where $\bar{n}_{1,2} = \sum_{n_1,n_2} |\psi_{n_1,n_2}(t)|^2 n_{1,2}$.
The results illustrate the TIP delocalization effect [6] in a strongly disordered chain. This effect is a consequence of the mixing by the interaction of free boson states close in energy, delocalizing the TIP system in the free boson basis. Since the one body states are localized, this delocalization in the free boson basis also means delocalization in real space.
While the two particles without interaction are confined to a localization domain in the random potential which is very quickly reached (typically for $t \approx 200$), at $U = 1$ the center of mass becomes delocalized [4]. This TIP ellipsoidal localization domain is reached and stops to spread after a considerably larger time (typically for $t \approx 5.10^4$). For a given sample, one can see that $|\psi_{n_1,n_2}(t = 5.10^4)|^2$ does not homogeneously fill the ellipse, and is characterized by large fluctuations, mainly near the border of the ellipse [4]. These fluctuations are somewhat similar to those characterizing the interaction matrix elements coupling the free boson states (see Sec. 1.2 and Ref. [2]).
We now study the intermediary time scales during which the center of mass $R(t)$ spreads, before the time t_2 where it saturates and TIP localization occurs. For $U = 0$, the aspect ratio $R(t)/\rho(t)$ of $|\psi_{n_1,n_2}(t)|^2$ remains equal to one at all times, but for $U \neq 0$, the time evolution of this ratio exhibits three regimes (Fig. 4), delimited by two characteristic time scales t_1 and t_2. For $t \leq t_1$, the repulsive interaction favors $\rho(t)$ and de-favors $R(t)$. The ratio $R(t)/\rho(t)$ decreases. This is the ballistic regime characterizing length scales smaller than L_1. The situation is opposite for $t_1 < t < t_2$ where L_1 has been reached and the interaction assisted propagation of the center of mass begins, on scales larger than L_1. The increase of $R(t)$ is now much faster than the increase of $\rho(t)$, and the ratio $R(t)/\rho(t)$ increases. L_2 is reached at $t = t_2$ where TIP localization occurs.
For $t \leq t_1$ we find that the spreading of the center of mass is almost ballistic yielding $R(t) \sim v(U)t^{\mu(U)}$ with $\mu(U) \approx 1$ and that the interaction reduces the increase of $R(t)$.
The time evolution strongly depends on the initial condition. When the two particles are injected on the same site at $t = 0$, with an energy of order U, the spreading of the center of mass is almost suppressed by a too large interaction. This is the dynamics associated to the molecular states $|nn\rangle$, which do not decay when U becomes very large [3, 4].

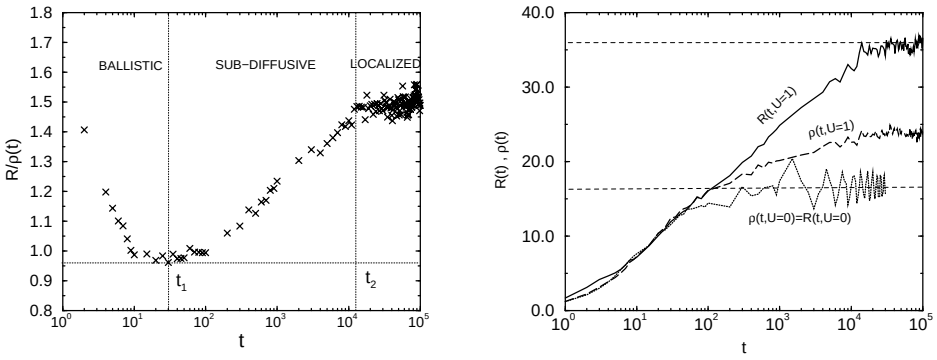

Fig. 4: Single sample with $L_1 = 16, L = 1024$ and $U = 1$. Left: $R(t)/\rho(t)$. Right: $R(t)$, $\rho(t)$ and $\rho(t)$ for $U = 0$ and $U = 1$.

On the contrary, injecting the two particles at two neighboring sites (0 and $\rho_0 = 2$) with an energy close to $E = 0$, one can see the dynamics associated to the hard core boson states and the consequence of the duality relation $U \leftrightarrow 1/U$ between the free bosons and the hard core bosons [4]. Averages over the random potential at different times clearly confirm that the duality appears in the quantum dynamics of $R(t)$ for both, the ballistic and the sub-diffusive regime [4].
To define the characteristic time t_1 separating the ballistic and sub-diffusive regimes, one can use many criteria. For instance, t_1 can be defined (i) as the time $t_1^{\min}$ where the minimum of $R(t)/\rho(t)$ is reached (see Fig.4); (ii) as the time scale t_1^s allowing to map the curves $R(t)/\rho(t)$ onto a single scaling curve $R(t)/\rho(t) = f_s(t/t_1^s)$. The existence of such a scaling is shown in Fig. 5, the resulting time being $\frac{t_1}{L_1} = f(U) \approx 1 - 0.3U$. We have checked that the definitions (i) and (ii) are compatible [4].

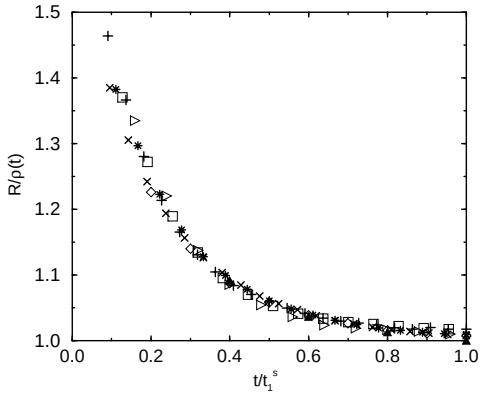

Fig. 5: Rescaling $R(t/t_1^s)$ with $L_1 = 24$ $U = 0.5$ (pluses), $U = 1$ (squares), $U = 1.5$ (diamonds), $U = 2$ (full triangles) and $U = 1$ $L_1 = 16$ (triangles), $L_1 = 36$ (stars), $L_1 = 50$ (crosses).

The interesting feature of $t_1^{\min}$ is that $R \approx \rho$ at this time, as when $U = 0$. This time where the effect of the interaction is inverted should be related to the size L where the TIP level curvature (see Section 1.4 and Ref. [5]) does not depend on U.
After the ballistic propagation for $t < t_1$, the spreading of the center of mass measured by $R(t)$ saturates without interaction. This is due to one particle quantum interferences yielding one particle Anderson localization. When $U \neq 0$, this saturation is suppressed, but the spreading $R(t)$ has now a so slow increase that a logarithmic scale for the time t is appropriate.
For the relative separation $\rho(t)$ between the two particles, the prediction $\rho(t) \approx L_1(1+\ln(\Gamma_1 t))$ [26] is in good agreement with the numerical results [4]. The evolution of the center of mass is on the contrary not described by the (modified) diffusion law $R(t) \approx \sqrt{D_2(t)t}$, but has a much slower logarithmic motion $R(t) \propto \log(t)$. This observation is related [4] to the multifractality of the interaction matrix elements in one dimension and the critical statistics observed at $L = L_1$.

1.4 Level curvatures

We now discuss the sensitivity of the TIP energy levels with respect to a magnetic flux φ enclosed by a one-dimensional ring. This yields additional informations on the quantum dynamics [5]. The flux appears in the phase of the hopping elements $t = t_0 \exp(2\pi i\phi/L)$. The dimensionless flux $\phi = \varphi/\varphi_0$ with the flux quantum $\varphi_0 = hc/e$. For the one-particle case the curvatures $c_\alpha = \partial^2\epsilon_\alpha/\partial\phi^2\big|_{\phi=0}$ of the eigenvalues ϵ_α of H_1 are directly related to the conductance by means of the Thouless relation.
The absolute values of the curvatures of different levels (even within the same disorder realization) usually differ by many orders of magnitude, making it difficult to obtain reliable numerical results for small as well as for large curvatures. Therefore we calculate the two-particle eigenenergies at several values of the magnetic flux between $\phi = 0$ and $\phi \sim 10^{-3}$. For each of the M eigenvalues, we first estimate the fourth derivative with respect to the flux. Then, we perform a least square fit with a parabola to the calculated data. The weights of the data points at different flux values are adjusted individually for each of the eigenvalues as a function of the estimates for the fourth derivative and the typical inaccuracy of the numerically calculated eigenvalues [27].
Since we want to discuss typical values of the curvatures as a function of disorder and interaction strength, the averaging technique must be chosen carefully. We found that the most reproducible results for typical curvatures are obtained by fitting the distribution of curvatures (rather than computing averages) because this minimizes the influence of the statistically less accurate points in the tails of the distribution. We always used a log-normal fit for this purpose, yielding numerically reliable results for the average $\langle \ln|c| \rangle$ and introduce $\tilde{c} = \exp(\langle \ln|c| \rangle)$ as a typical curvature [5].
Interactions have a significant influence on the typical two-particle level curvatures. This can be seen by comparing the open symbols in Fig. 6 (which are for $U = 0.5$) to the non-interacting case given by the full symbols. The influence of the interaction is shown for disorder strengths $W = 0.75$ and $W = 1.5$. The main observation is that while at low disorder interactions decrease the curvatures, the latter are increased at higher disorder when the one-particle states are localized. This is a direct confirmation of the prediction by Akkermans and Pichard [14]. A closer look at the data reveals a strong dependence of the effect on the energy regime with a tendency to remove the dip in the curves around $E = 0$.

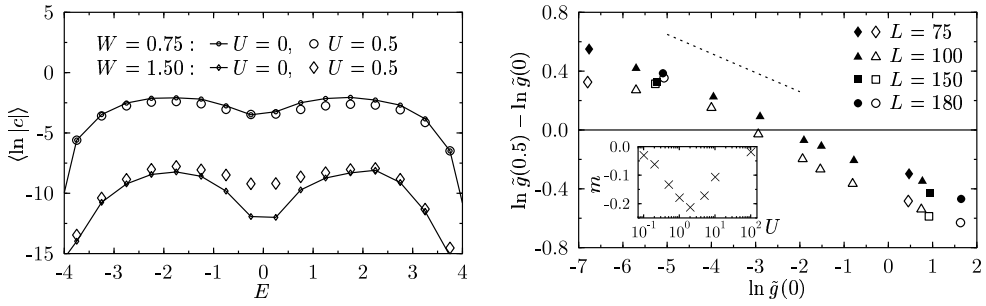

Fig. 6: Left: The energy dependence of typical curvatures for different disorder strengths W and $L = 100$. $\langle \ln |c| \rangle$ is plotted for the cases without (full symbols, connected by lines) and with interaction $U = 0.5$ (open symbols). Right: The difference of the logarithms of the dimensionless curvatures $\tilde{g}(U)$ at interaction strength $U = 0.5$ and $U = 0$ versus the logarithm of $\tilde{g}(0)$. Full symbols represent the energy range $[-2.5 : -1]$, open symbols $[1 : 2.5]$. Different ring sizes $L = 75$ with $W = 0.9$ and $W = 1.8$, $L = 100$ with W between 0.75 and $W = 1.5$, $L = 150$ with $W = 0.6$ and $W = 1.2$, $L = 180$ with $W = 0.45$ and $W = 1.1$. The dotted line has the same slope $m \approx -0.13$ as the scaling curves. The inset shows the dependence $m(U)$ of this slope on the interaction strength U.

Since the influence of the interaction depends on the mobility of the particles (increase for localized, decrease for metallic samples), it is tempting to define a dimensionless curvature $\tilde{g}(U) = \tilde{c}/\Delta_1$ where $\tilde{c}$ is the typical curvature at interaction U and $\Delta_1 \approx 2(2t_0 + W)/L$ is the mean one-particle level spacing, and to plot the interaction-induced change of curvatures over the conductance-like parameter $\tilde{g}(0)$.
In Fig. 6, the difference between the logarithms of the typical absolute values of the dimensionless curvatures with interaction $U = 0.5$ and without interaction are plotted versus the logarithm of the conductance-like parameter $\tilde{g}(0)$ in the energy intervals $[-2.5 : -1]$ and $[1 : 2.5]$, for different ring sizes and disorder strengths W. We have considered also other energy values [5] and conclude that the interaction-induced change of the curvatures depends not on the energy and the disorder separately, but on only one parameter which is indeed the conductance-like $\tilde{g}(0)$. This one-parameter scaling is universal within a given sign of the energy. No change of the scaling curves is observed when the ground state energy is approached. This means that the effect is relevant also for energetically low-lying excitations relevant for transport at low temperatures. This is consistent with the findings of Ref. [28, 29].
Our results clearly demonstrate the existence of a critical $\tilde{g}(0) = \tilde{g}_{\rm crit}$ below which the interaction enhances two-particle level curvatures, and above which the interaction tends to decrease the typical curvatures. Since the level curvature without interaction is related to the conductance of the system, this clearly confirms that the sign of the interaction-induced change indeed depends on the transport properties of the non-interacting system as predicted [14]. With an estimate of the typical one-particle curvature one finds that the critical conductances observed correspond to localization lengths L_1 which are about 5 to 6 times smaller than the circumference of the ring [5]. Lower conductances $\tilde{g}(0) < \tilde{g}_{\rm crit}$ correspond to localized states and the enhancement of the curvatures is a consequence of the enhancement of the two-particle localization length by the interactions proposed by Shepelyansky [6]. Larger conductances $\tilde{g}(0) > \tilde{g}_{\rm crit}$ can be interpreted as indicating more or less extended one-particle states for

which the transport is suppressed by the interactions.
Within the numerical errors, the data lie on the scaling curve which corresponds to their sign of energy. In the logarithmic representation shown in Fig. 6 the scaling curves are very close to straight lines. The slopes $m(U)$ vary between $m = 0$ (at $U = 0$ and $U = \infty$) and the minimal value $m \approx -0.2$ at intermediate interaction strength. The behavior of $m(U)$ (inset of Fig. 6) shows again the duality relation (Section 1.1 and Ref [3]).
The behavior of the curvatures is closely related to what is found for the dynamics of two-particle wave-packets (Section 1.3 and Ref. [4]). The interaction leads to a slower spreading at short times, before L_1 is reached. For these short times, only a part of the system smaller than L_1 is explored by the particles and their reduced mobility corresponds to the decrease of the curvature in the metallic regime ($L < L_1$) when $\tilde{g}(0)$ is large. Above a characteristic time t_1, a slow interaction assisted propagation continues to increase the size of the wave-packet beyond the non-interacting saturation. This is reminiscent of the increase of curvatures in insulating samples ($L > L_1$) when $\tilde{g}$ is small.
Having considered also the effect of long-range interactions, we found that the range of the interaction has only a very small influence on the typical curvatures, as compared to the difference between $U = 0$ and short-range interaction [27]. This may yield problems in a possible experimental verification [30] of the delocalization effect at strong disorder as a function of the range of the interaction.
Additionally, it was found that not only the typical value of the two-particle level curvatures but also their probability distribution $P(|c|)$ changes as a function of the interaction [5].

2 Charge reorganization and Delocalization of the ground state for a finite density of spinless fermions

So far, we have considered two particle states close to the TIP band center, at energies much higher than the TIP ground state. At those energies, the TIP levels are very dense, with energy spacings of order $\Delta_2 \approx 4t/L^2$. The mixing by the interaction and the resulting delocalization effect can be strong. For the finite density system, one may assume a Fermi gas and quasi-particle excitations. In this hypothesis, the density of two quasi-particles above the Fermi sea is much lower at small excitation energy ϵ, with energy spacings of order $\Delta_2^{qp}(\epsilon) \approx \Delta_1^2/\epsilon$ instead of Δ_2. $\Delta_1 \approx 2t/L$ denotes the one particle spacing. Our previous study applies for very high excitation energies $\epsilon \approx t$ where $\Delta_2^{qp} \approx \Delta_2$. This point of view assumes that the ground state itself cannot be reorganized by the interaction. For a strong enough disorder, one should however expect such a reorganization. Without interaction, one has an Anderson insulator (Fermi glass) characterized by an inhomogeneous charge configuration: strongly localized states are populated with the restriction imposed by Pauli principle. For a strong interaction, one has a Mott insulator (or a pinned Wigner crystal for long range Coulomb interaction) characterized by a more homogeneous periodic charge configuration, slightly distorted by the random substrate. The crossover between those two limits will yield a profound spatial reorganization of the ground state [28], making the system more sensitive to any external perturbation as a twist in the boundary conditions or a flux Φ in a ring.
To illustrate this, we consider N spinless fermions on a chain of L sites with nearest

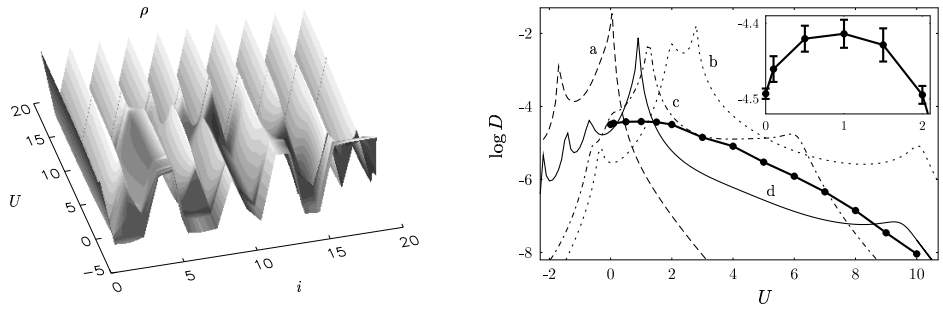

Fig. 7: Left: Charge configuration for a typical sample (d) for $N = 10$ particles on $L = 20$ sites at $W = 4.5$. Right: Phase sensitivity $D(U)$ for four different samples with $N = 10$, $L = 20$ and $W = 4.5$ in (decimal) logarithmic scale. Thick dots and inset: average of $\log(D)$.

neighbor (NN) interaction

$$H = -t \sum_{i=1}^{L} (c_i^\dagger c_{i-1} + c_{i-1}^\dagger c_i) + \sum_{i=1}^{L} V_i n_i + U \sum_{i=1}^{L} n_i n_{i-1}$$

and twisted boundary conditions, $c_0 = \exp(i\Phi) c_L$. The operators c_i ($c_i^\dagger$) destroy (create) a particle on site i and $n_i = c_i^\dagger c_i$ is the occupation operator. The on-site random energies V_i are drawn from a box distribution of width $2W$. The strength of the disorder W and the interaction U are measured in units of the kinetic energy scale ($t = 1$). We study interaction between NN at half filling, where the ground state will be a periodic array of charges located on the even or odd sites of the chain when $U \to \infty$.

The numerical results are obtained with the density matrix renormalization group (DMRG) algorithm [31]. Ground state properties in disordered $1d$ systems can be calculated with an accuracy comparable to exact diagonalization, but for much larger systems (we keep up to 2000 states per block [33]).

The reorganization of the ground state induced by the NN repulsion is shown in Fig. 7, where the density ρ (expectation value of n_i) is plotted as a function of U and site index i. To favor the inhomogeneous configuration, the disorder is taken large ($W = 4.5$) and $L_1 \approx 25/W^2$ is of order of the mean spacing $k_{\rm f}^{-1} = 2$ between the charges. For $U \approx 0$, one can see a strongly inhomogeneous and sample dependent density, while for large U a periodic array of charges sets in. These two limits are separated by a sample dependent crossover regime. For certain random configurations, the periodic array is quickly obtained by a weak repulsive interaction, while one needs a strong interaction for other samples.

To measure the delocalization effect associated to this change of configuration, we study the phase sensitivity of the ground state. The energy difference between periodic ($\Phi = 0$) and anti-periodic ($\Phi = \pi$) boundary conditions, $\Delta E = (-)^N (E(0) - E(\pi))$ conveys similar information, in the localized regime, as other measures of the response of the ground state to an infinitesimal flux threading the ring: the Kohn curvature (charge stiffness) $\propto E''(\Phi = 0)$ and the persistent current [1] $J \propto -E'(\Phi = 0)$. For strictly $1d$ systems, the sign of $E(0) - E(\pi)$ simply depends on the parity of N, and the factor $(-)^N$ makes ΔE positive.

The phase sensitivity $D(U) = (L/2)\Delta E$ is shown in Fig. 7 for four samples at half

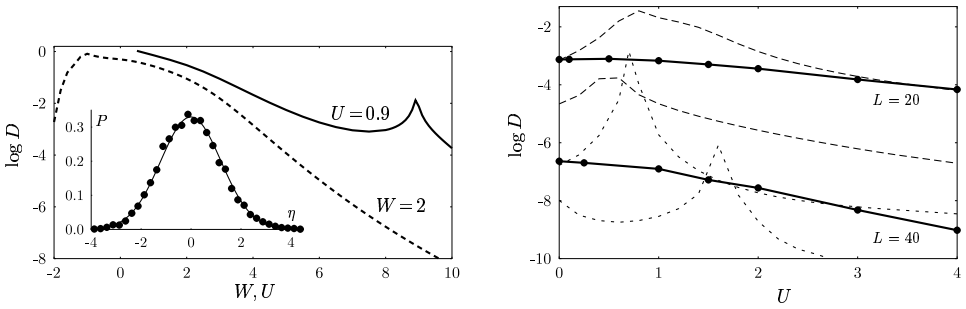

Fig. 8: Left: Phase sensitivity for the sample d of Fig. 7. Solid: $D(W)$ at $U=0.9$; dashed: $D(U)$ at $W=1$. Inset: Probability distribution (dots) of $\eta=\log D(2)-\log D(0)$ calculated from 10000 samples ($L=20$, $N=10$, $W=4.5$) fitted by a Gaussian with variance $\sigma^2=1.46$. Right: Phase sensitivity $D(U)$ for $L=20$ and $L=40$ at half filling and disorder $W=3.5$. Dashed lines with stars and diamonds represent two individual samples at $L=20$, dotted lines are for the lengthened samples at $L=40$. Thick dots and solid lines are the averages over a large number of samples.

filling with $W=4.5$. Both for $U\approx 0$ and $U\gg 1$, $D(U)$ is very small, but sharp peaks appear at sample dependent values U_c, where $D(U_c)$ in certain samples can be 4 *orders of magnitude larger than for free fermions*. Remarkably, the curves for each sample do not present any singularity at $U=0$ which could allow to locate the free fermion case. Peaks can be seen at different sample dependent values of U (positive or negative). For small repulsive interactions, the system is an Anderson insulator delocalized by U, and $D(U)$ increases as a function of U.

At U_c, the regular array of charges is established, and thereafter it becomes more and more rigid (pinned by the random lattice); thus $D(U)$ decreases as a function of U. The thresholds U_c are strongly sample dependent giving rise to a very wide distribution of $D(U)$: the ensemble average at a given U mixes very different behaviors and provides very incomplete information. As shown in Fig. 7, $\langle \log D(U)\rangle$ decreases for repulsive interactions, except for a small interval around $U\approx t$ (inset) where a local maximum is obtained.

We obtain log-normal distributions for $D(U)$ as well as for the difference $\eta=\log D(U)-\log D(0)$ that measures the relative change of the phase sensitivity with respect to the free fermion case. The width of the η-distribution depends on U. For $U=2$ variations of D over more than an order of magnitude are typical (inset of Fig. 8).

This delocalization effect of the ground state for $U=t$ only occurs at strong disorder. For weak disorder ($W=1, L_1\approx M$) we recover the behavior expected starting from the clean limit, using bosonization and renormalization group arguments [32, 33]: a repulsive interaction reinforces localization, in contrast to a (not too strong) attractive interaction which delocalizes (Fig. 8). Fixing $U=0.9$, we show (in the same graph) how one goes from the weak to the strong disorder limit in a given sample (the same seed of the random number generator is kept). The phase sensitivity decreases when we increase the strength of the potential fluctuations, except around $W=4.5$ ($k_{\rm f}l\approx 1$) where the charge reorganization takes place. The conclusion that a repulsive interaction favors localization is no longer valid. Similar conclusions have been drawn from a study of the conductance of one- and two-dimensional systems at half filling [29].

One may suspect that going to samples longer than those we have presented so far induces a certain amount of self-averaging, thus reducing the effect of the charge reorganization. We have addressed the problem of the thermodynamic limit by considering a sample of length L, and then putting in series another segment with the same length and an independent impurity potential, thereby keeping the electron density constant. Such a study is presented in Fig 8, where the phase sensitivity of two samples with $L = 20$ (think dashed and solid lines) is shown together with the corresponding $D(U)$ for $L = 40$ (thick dashed and solid lines). Doubling L and N typically shifts $\log D(U)$ four orders of magnitude below, except around the peaks, which are still present in the longer samples and become much sharper. In some samples additional structure, arising from the charge reorganization in the attached portion, may appear. Thus, the relative delocalization effect looks larger when the size is doubled. The complete study of the thermodynamic limit and the behavior of the localization length as a function of U is in progress.

3 Summary

For two interacting excited particles in a disordered one-dimensional chain, we obtained a consistent picture of a rich and complex behavior of the system as a function of the disorder and of the interaction for a fixed kinetic energy. The multifractal properties of the perturbation induced by the interaction or by the kinetic energy around the limits where $U \to 0$ or $U \to \infty$ respectively have the interesting consequence that the TIP spectrum can never have spectral statistics more rigid than critical statistics connected with weak quantum chaos. These maximum correlations are accompanied by multifractal wave-functions and occur at an intermediate interaction strength. A duality transformation maps the two limits onto each other whose signature can be seen for many different quantities. Another consequence of the multifractal perturbation is the slow logarithmic sub-diffusive delocalization of the center-of-mass extension of wave-packets found in the real-time dynamics. Further, it becomes clear from studies of the level curvatures and the real-time dynamics of wave-packets that the interactions improve transport only in the regime where one-particle wave-functions are localized. In the metallic regime, they rather decrease the mobility of the particles.

From a DMRG study of the ground state of spinless fermions with NN interactions at half filling, we draw a few important conclusions.

(i) Each sample should be individually studied. The (log)-averages over the ensemble are not representative. The distribution of $\ln D(U)$ is very broad, fluctuations of a few orders of magnitude being observed in the studied case.

(ii) The ratio $L_1/(L/N)$ (say $k_{\rm f}l$) defines different regimes for short-range repulsive interactions. For $k_{\rm f}l > 1$, the interaction establishes a correlated array of charges inside L_1 which is pinned by the random lattice. The larger is U, the more rigid is the array, the more efficient is the pinning and the system is strongly insulating (Mott). When $k_{\rm f}l < 1$, the particles can be strongly localized far away from each other, and a short range interaction does not affect a strongly insulating ground state (Fermi glass). Only very excited quasi-particles can be delocalized by the interaction. Between those two limits, $k_{\rm f}l \approx 1$, the ground state can be deeply reorganized by a repulsive interaction $U \approx t$. This reorganization is accompanied by a large delocalization effect.

In the two studied cases, we obtain an interaction induced delocalization for intermediate strengths of the interaction, in a crossover regime between two "integrable"

limits with Poisson spectral statistics: free bosons and hard core bosons for the TIP problem, Fermi glass and Mott insulator for the ground state at half filling. Eventually, the spins should not be frozen as assumed in this study. For instance, for two interacting electrons, the crossover between the free fermions and the hard core bosons may be artificial. We should rather expect an interesting magnetic crossover induced by the interaction. Around U_c, the two opposite spins should flip and become parallel, the orbital wave function becoming antisymmetric. In our case, imposing opposite spins, we have been obliged to resymmetrize artificially the Slater determinants (hard core bosons). A study taking into account possible spin effects is in progress.

References

[1] *Correlated Fermions and Transport in Mesoscopic Systems*, Proc. XXXI. Rencontres de Moriond, ed. by T. Martin, G. Montambaux and J. Trân Thanh Vân, Editions Frontières (Gif-sur-Yvette 1996).

[2] X. Waintal and J.-L. Pichard, TIP I, cond-mat/9706258, to appear in Eur. Phys. J. B.

[3] X. Waintal, D. Weinmann, J.-L. Pichard, TIP II, cond-mat/9801134, to appear in Eur. Phys. J. B.

[4] S. De Toro Arias, X. Waintal, J.-L. Pichard, TIP III, cond-mat/9808136.

[5] A. Wobst and D. Weinmann, TIP IV, cond-mat/9808138, to appear in Eur. Phys. J. B.

[6] D. L. Shepelyansky, Phys. Rev. Lett. **73**, 2067 (1994).

[7] Y. Imry, Europhys. Lett. **30** 405 (1995).

[8] Ph. Jacquod and D.L. Shepelyansky, Phys. Rev. Lett. **75**, 3501 (1995).

[9] B.I. Shklovskii, B. Shapiro, B.R. Sears, P. Lambrianides and H.B. Shore, Phys. Rev. B **47**, 11487 (1993).

[10] V.I. Fal'ko and K.B. Efetov, Europhys. Lett. **32**, 627 (1995); Phys. Rev. B **52**, 17413 (1995).

[11] K. Frahm, A. Müller-Groeling, J.-L. Pichard, D. Weinmann, Europhys. Lett. **31**, 169 (1995).

[12] J.T. Edwards, D.J. Thouless, J. Phys. C **5**, 807 (1972).

[13] D.J. Thouless, Phys. Rep. **13**, 93 (1974).

[14] E. Akkermans and J.-L. Pichard, Eur. Phys. J. B **1**, 223 (1998).

[15] I.V. Ponomarev and P.G. Silvestrov, Phys. Rev. B **56**, 3742 (1997).

[16] B.L. Altshuler, Y. Gefen, A. Kamenev and L.S. Levitov, Phys. Rev. Lett. **78**, 2803 (1997).

[17] G. Paladin and A. Vulpiani, Phys. Rep. **156**, 147 (1987).

[18] T.C. Halsey, M.H. Jensen, L.P. Kadanoff, I. Procaccia and B.I. Shraiman, Phys. Rev. A **33**, 1141 (1986).

[19] D. Weinmann and J.-L. Pichard, Phys. Rev. Lett. **77**, 1556 (1996).

[20] D. Weinmann, J.-L. Pichard and Y. Imry, J. Phys. I (France) **7**, 1559 (1997).

[21] M. Leadbeater, R.A. Römer, M. Schreiber, cond-mat/9806255.

[22] A. Bohr and B. R. Mottelson, Vol. 1, Appendix 2-D, *Nuclear Structure*, Benjamin, New York (1969).

[23] E. Bogomolny, U. Gerland and C. Schmit, IPN-Orsay preprint.

[24] Ph. Jacquod and D.L. Shepelyansky, Phys. Rev. Lett. **79**, 1837 (1997).

[25] S. De Toro Arias and C. Vanneste J. Phys. I France **7**, 1071 (1997).

[26] K. Frahm, A. Müller-Groeling and J-L. Pichard Phys. Rev. Lett. **76**, 1509 (1996); Z. Phys. **B** 102, 261 (1997).

[27] A. Wobst, Diplomarbeit, Universität Augsburg (1998).

[28] P. Schmitteckert, R.A. Jalabert, D. Weinmann, J.-L. Pichard, Phys. Rev. Lett. **81**, 2308 (1998).

[29] T. Vojta, F. Epperlein, M. Schreiber, cond-mat/9806194; M. Schreiber, F. Epperlein, T. Vojta, cond-mat/9807385.

[30] D. Brinkmann, J.E. Golub, S.W. Koch, P. Thomas, K. Maschke, I. Varga, Marburg preprint (1998).

[31] S.R. White, *Phys. Rev.* **B 48**, 10345 (1993).

[32] T. Giamarchi, H. Schulz, *Phys. Rev.* **B 37**, 325 (1988).

[33] P. Schmitteckert et al., *Phys. Rev. Lett.* **80**, 560 (1998).